


Locally self-consistent embedding approach for disordered electronic systemsYi Zhang ^{1,2,*}, Hanna Terletska,³ Ka-Ming Tam,^{1,2} Yang Wang,⁴ Markus Eisenbach,⁵ Liviu Chioncel,^{6,7} and Mark Jarrell^{1,2}¹Department of Physics and Astronomy, Louisiana State University, Baton Rouge, Louisiana 70803, USA²Center for Computation and Technology, Louisiana State University, Baton Rouge, Louisiana 70803, USA³Department of Physics and Astronomy, Middle Tennessee State University, Murfreesboro, Tennessee 37132, USA⁴Pittsburgh Supercomputing Center, Carnegie Mellon University, Pittsburgh, Pennsylvania 15213, USA⁵Center for Computational Sciences, Oak Ridge National Laboratory, Oak Ridge, Tennessee 37831, USA⁶Theoretical Physics III, Center for Electronic Correlations and Magnetism, Institute of Physics, University of Augsburg, D-86135 Augsburg, Germany⁷Augsburg Center for Innovative Technologies, University of Augsburg, D-86135 Augsburg, Germany

(Received 4 June 2019; revised manuscript received 18 August 2019; published 28 August 2019)

We present an embedding scheme for the locally self-consistent method to study disordered electron systems. We test this method in a tight-binding basis and apply it to the single band Anderson model. The local interaction zone is used to efficiently compute the local Green's function of a supercell embedded into a local typical medium. We find a quick convergence as the size of the local interaction zone which reduces the computational costs as expected. This method captures the Anderson localization transition and accurately predicts the critical disorder strength. The present work opens the path towards the development of a typical medium embedding scheme for the $O(N)$ multiple scattering methods.

DOI: [10.1103/PhysRevB.100.054205](https://doi.org/10.1103/PhysRevB.100.054205)**I. INTRODUCTION**

Disorder which is a ubiquitous feature of real materials (in the form of impurities or defects in perfect crystals, or chemical substitutions in alloys and random arrangements of electron spins or glassy systems) plays a key role in changing and controlling their properties [1–5]. As shown long ago by Anderson [6], disorder in atomic coordinates creates spatially confined or “localized” electron eigenstates near the Fermi level. Electron localization has been found to play a crucial role in a number of materials, starting from the prototype two-dimensional electron systems [7], displaying metal to insulator transitions [1], to various well-known semiconducting materials including Dirac [8–11] and Weyl [12–14] semimetals.

Among the well-known studied systems, are semiconductors such as Si doped with P, B, S, or Ti. For instance, in Si:P the P donors sit substitutionally on the Si sites and for low concentrations, according to Mott [15,16], there is a negligible overlap between the wave functions of the donor electrons, and the material is an insulator. At high concentrations when the overlap is large compared with the on-site repulsion the material is a metal. These observations led Mott [15,16] to formulate a phenomenological theory for the transition from the insulating to the metallic state (localized to itinerant electrons) in terms of a critical concentration n_c and the average distance between the impurities fulfilling the relation $n_c^{1/3} a_B \approx 1/4$, where a_B is the spatial extension (effective Bohr radius) of the P donor electrons. The alternative view due to Anderson [6] involves localization due to random one-electron poten-

tials seen by the electrons. For low donor concentrations the one-electron energy spread in the random potentials (energy distance between consecutive energy eigenstates) is large compared with the energy bandwidth and the electronic states are localized. At high concentrations, the localized impurity states form the impurity band and the extended states appear separated from the localized states by a mobility edge. The metal-insulator transition can also happen by doping which shifts the Fermi level across the mobility edge.

Dilute magnetic semiconductors (with a subtle interplay between magnetism and electron localization) and intermediate band photovoltaics (which hold the promise to significantly improve solar cell efficiency) are among another important class of materials where disorder plays a fundamental role on their properties. Dramatic improvement in crystal growth in recent years has enabled preparation of samples with a significant control over the degree of disorder. For example, localization has been definitively seen in single crystals of $\text{Li}_x\text{Fe}_7\text{Se}_8$ despite of a finite density of states at the Fermi energy confirmed via specific heat and reflectivity measurements [17]. Besides these systems, thermoelectric and topologic materials such as Cd_3As_2 , Na_3Bi [8–11], and TaAs , NbAs [12–14] hint towards the presence of significant disorder effects that still remain to be fully understood.

In recent decades, the *ab initio* methods based on density functional theory (DFT) [18–22] have become the most important tool to calculate properties of ordered crystalline solids. The band theory as such cannot be used to treat disordered solids because of the lack of translation invariance. For modeling disordered solids calculations were performed using effective medium theories, among them the coherent potential approximation (CPA) [23] proved to be a simple and transparent theory that is able to capture important features

*zhangyiphys@gmail.com

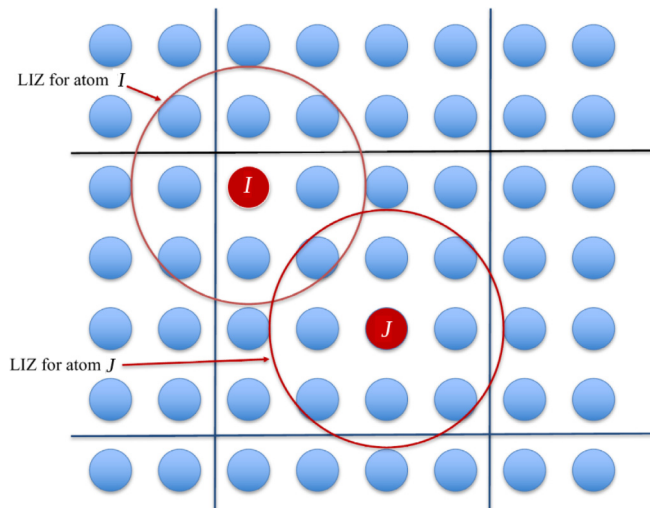


FIG. 1. A schematic representation of the LIZ (red circles), centered around the sites I, J .

of the electronic structure of alloys. The CPA has been used to solve models which helped in providing physical interpretation of experimental results on real alloys. To become quantitative the CPA equations have been formulated for the muffin-tin potentials within the multiple-scattering Korringa-Kohn-Rostocker method [24,25]. The configurational average could be performed over the scattering path operator, instead of the Green's function (used for models), simplifying the implementation of the CPA for materials calculations [26]. Later the CPA was also implemented within the linearized muffin-tin orbitals [27] basis set [28–31]. With the advent of the third-generation exact muffin-tin orbitals [32–34] method, and the full-charge density [35] technique, it was possible to go beyond the atomic-sphere approximation with CPA calculations [36], and investigate the energetics of anisotropic lattice distortions.

An alternative to the effective medium theories is supercell calculations which nowadays can be performed on systems containing thousands of atoms. This has been made possible by the development of order- N [$O(N)$] methods based on plane-wave expansions [37,38] or multiple-scattering theory [39]. In the multiple-scattering formulation the linear scaling *ab initio* method came to be known as the locally self-consistent multiple scattering (LSMS) method. LSMS achieves linear scaling for very large systems with up to tens of thousands of atoms, via the introduction of a smaller local interaction zone (LIZ) of size N_{LIZ} of several hundreds of sites. Within the LIZ the electronic structure problem is solved explicitly with free space boundary conditions. In LSMS analysis, as the LIZ moves through each site, the explicit DFT solution introduces correlations due to the different disorder configuration (Fig. 1).

In this paper, we present our concept of embedding that combines the real space construction with the momentum space self-consistency. In this scheme we follow the ideas of LSMS implementation [39] and investigate electron localization in a three-dimensional (3D) Anderson model. This represents a natural extension of our previous study on multiple-scattering formulation to the problem of Anderson

localization [5]. However, contrary to standard LSMS, our scheme does not explicitly rely on the multiple-scattering aspect of the cluster solver. In comparing the results obtained using the local average coherent potential and typical effective medium embedding schemes, we find that the typical medium embedding plays a significant role in capturing electron localization [40,41]. In particular, the extrapolated critical disorder strength for the Anderson transition is in excellent agreement with the known literature results [42–49].

The remainder of this paper is organized as follows. After the introduction, we discuss some conceptual details of LSMS in Sec. II, followed by the typical medium formulation of the Anderson localization in Sec. III. In Sec. IV, we present the computational details and the self-consistent loop used in the present calculations. Then in Sec. V we illustrate the effective medium embedding using the Hamiltonian formulations and present results for the coherent potential effective medium and the typical medium.

II. CALCULATING PROPERTIES WITH LSMS

LSMS has the unique capability to study extremely large and disordered systems [50,51]. Yet, the standard construction of the LIZ using an open boundary condition limits the applicability of LSMS to the description of disordered metals only, and in particular fails to properly describe band gaps and electron localization. This is because free space boundary conditions, for which the potential is set to be zero, couple the LIZ to a free space density of states which increases as a square root for positive energies, so that the gaps in a semiconducting system are filled in and blurred, and semiconductors appear to be metals. One possible way to overcome this issue is to use self-consistently determined boundary conditions. Inspired by the LSMS construction, Abrikosov *et al.* [40,41] suggested a locally self-consistent method in which the LIZ size is reduced by considering an effective scatterer outside the LIZ. The choice made for this scattering matrix is the CPA single-site t matrix. The excellent convergence achieved through this method [30,40,41] allowed one to also address the problems of total energy calculations in alloys [52–54].

Note that the open boundary conditions imposed upon an LIZ also disable the ability of LSMS to study electron localization. It has been shown recently [5,55] that the average density of states (DOS) is not critical through the Anderson transition, and instead the typical (geometrically averaged density of states) needs to be used to identify the transition [55]. Therefore, in order to capture the electron localization in real materials using the LSMS scheme, the boundary conditions must couple the LIZ to an effective medium which reflects the typical order parameter. The essential aspects of the typical medium theory are discussed in the following section.

III. TYPICAL MEDIUM APPROACH

Recent studies [5,55] have shown that disorder-driven electron localization is captured by typical medium approaches. The typical medium approach takes into account the dramatic changes of the distribution of the local density of states (LDOS) through the localization transition. More specifically,

it changes from a Gaussian distribution to a skewed log-normal distribution, where the algebraic average of the LDOS stays finite while the geometric average of the LDOS which is usually called the typical density of states (TDOS) drops to zero [56]. This property of TDOS makes it a potential candidate order parameter for the localization transition. Typical medium analysis helps to overcome the shortcomings of the standard effective medium methods such as CPA [23] and dynamical cluster approximation (DCA) [57] which fail to describe the localization transition. The typical medium theory (TMT) introduced for the first time by Dobrosavljević *et al.* [55], successfully captures precursors of the Anderson localization transition, but strongly overestimates the localization effect due to its single-site nature. Later, a finite size cluster extension of TMT, the so-called TMDCA, was introduced [5] which accurately predicts the critical disorder strength of the Anderson localization transition in a single-band Anderson model with uniform disorder. The TMDCA has been extended to systems with off-diagonal disorder [58] and to multiband systems [59] in model Hamiltonians, where it accurately reproduces the localization phase diagrams. The obtained results are in agreement with other well-established theoretical techniques such as the transfer matrix and the kernel polynomial methods [58,59]. More recently, TMDCA was also combined with the first-principles calculations to study the localization effects in realistic materials with disorder [60–62]. The TMDCA formulated within the multiscattering theory is still used at the model Hamiltonian level [63].

IV. EMBEDDING SCHEME

In this section, we describe the construction of the effective medium embedding scheme using concepts of LSMS. The self-consistent embedding is a coupling framework which provides rigorous boundary conditions for the primary region (site, or cluster) to be embedded into a larger self-consistently determined environment. Central to the embedding theory is the embedding potential (e.g., a self-energy) which embodies the functional connection between the primary region and the environment. In the original LSMS calculation no embedding scheme is used, in other words, the LIZ was effectively embedded in a vacuum [39]. Later it has been shown that the size of the LIZ and hence the computational effort may be considerably reduced by embedding the LIZ in an effective medium [40]. Using the CPA as the embedding effective medium leads to the so-called locally-self-consistent Green's function method [41] which was applied to the metallic alloys. On the contrary, as will be shown below, the embedding into the effective typical medium allows one to address the Anderson localization transition.

In the following we describe our computational scheme. We first surround a site I_c of the lattice and form the LIZ (red circle of Fig. 2). Sites within the LIZ are denoted by capital letters (I, J) . We choose the LIZ of linear dimension L_{LIZ} to be contained in a supercell of dimension $L_c > L_{LIZ}$ [64]. The local interaction zone will be moved through all sites of the supercell. The supercell is repeated to restore the lattice translation invariance, generating the set of K points. Given a supercell Green's function $\bar{G}(\omega, K)$ the Fourier transform

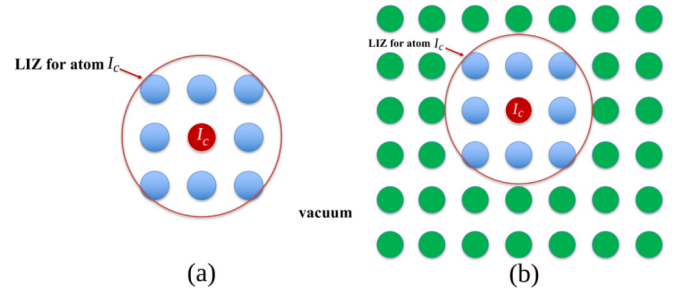


FIG. 2. Setups of the LIZ for conventional LSMS without embedding (a), and with embedding scheme (b). The index I_c denotes the center of the LIZ. Blue circles represent sites inside the LIZ while the green circles represent the homogeneous effective medium.

provides the real space Green's function in the supercell:

$$\bar{G}_{IJ}(\omega) = \frac{1}{N_c} \sum_K e^{iKR_{IJ}} \bar{G}(\omega, K), \quad (1)$$

where K are the supercell wave numbers, with N_c the number of sites in the supercell, defined in the same way as those in DCA [57]. The indices (I, J) cover all lattice sites within the supercell. The corresponding LIZ Green's function has the form

$$\bar{G}_{IJ}^{LIZ}(\omega) = \frac{1}{N_c} \sum_K e^{iKR_{IJ}} \bar{G}(\omega, K), \quad (I, J) \in \text{LIZ}, \quad (2)$$

where $\bar{G}(\omega, K)$ is defined through the coarse-graining procedure as

$$\bar{G}(\omega, K) = \frac{N_c}{N} \sum_{\tilde{k}} \frac{1}{\omega - \epsilon(K + \tilde{k}) - \Sigma_I(\omega)}. \quad (3)$$

The local effective self-energy is denoted by $\Sigma_I(\omega)$ and $\epsilon(K + \tilde{k})$ is the lattice dispersion. The supercell wave numbers K correspond to the N_c cells that divide the first Brillouin zone equally. The wave numbers \tilde{k} label the wave numbers within each cell surrounding K . The supercell is embedded into the effective medium, represented by Σ_I present at all supercell sites. Therefore, LIZ sites (contained in the supercell) experience the presence of the effective medium. Consequently, we may rewrite the real space LIZ Green's function $\bar{G}^{LIZ}(\omega)$ in the following form:

$$\underline{\bar{G}}^{LIZ}(\omega) = [\omega \cdot \underline{\mathbb{1}} - \underline{t}' - \underline{\Sigma}_I(\omega) \cdot \underline{\mathbb{1}} - \underline{\Gamma}^{LIZ}(\omega)]^{-1}. \quad (4)$$

The underline indicates matrices of dimension $L_{LIZ} \times L_{LIZ}$ corresponding to the number of sites contained within the LIZ. The hopping matrix elements within the LIZ are given by (\underline{t}') , and $\underline{\mathbb{1}}$ is the corresponding identity matrix. The hybridization function between the LIZ and the effective medium is $\underline{\Gamma}^{LIZ}(\omega)$ and the LIZ excluded Green's function can be defined as

$$\underline{\mathcal{G}}(\omega) = [\omega \cdot \underline{\mathbb{1}} - \underline{t}' - \underline{\Gamma}^{LIZ}(\omega)]^{-1}. \quad (5)$$

We do not explicitly evaluate the hybridization function $\underline{\Gamma}^{LIZ}(\omega)$; instead we directly calculate the LIZ excluded Green's function using

$$\underline{\mathcal{G}}^{-1}(\omega) = [\underline{\bar{G}}^{LIZ}(\omega)]^{-1} + \underline{\Sigma}_I(\omega) \cdot \underline{\mathbb{1}}. \quad (6)$$

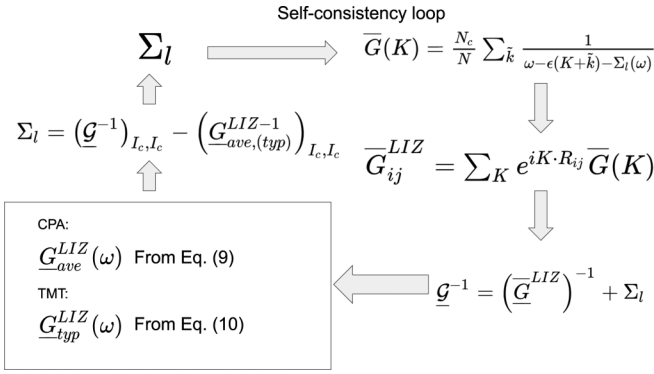


FIG. 3. The self-consistency loop for the CPA/TMT embedding method.

Here $\underline{G}(\omega)$ is the real space Green's function inside the LIZ in the absence of disorder. Accordingly, $\underline{G}(\omega)$ takes the same values for all possible LIZs obtained by running the center of the LIZ (I_c) through each sites in the supercell. Within the supercell we include the disorder potential, and we calculate the Green's function within each LIZ centered around the site I_c :

$$[\underline{G}^{LIZ}(\omega, V, I_c)]^{-1} = \underline{g}^{-1}(\omega) - \underline{V}(I_c), \quad (7)$$

where $\underline{V}(I_c)$ is a diagonal matrix of size N_{LIZ} . Note that the matrix $\underline{G}^{LIZ}(\omega, V, I_c)$ has the same dimension. The index I_c (the center of the LIZ seen in Fig. 2) serves also as an additional label indicating the presence of disorder at that specific site.

We average $\underline{G}^{LIZ}(\omega, V, I_c)$ over the different LIZ realizations within the supercell, which is expressed as $\frac{1}{N_c} \sum_{I_c} (\dots)$ and over the disorder configurations, which is indicated by the angle brackets $\langle \dots \rangle_V$. We employ two types of averaging, for the effective medium:

(1) Linear average (CPA):

$$\underline{G}_{ave}^{LIZ}(\omega) = \frac{1}{N_c} \sum_{I_c} \langle \underline{G}^{LIZ}(\omega, V, I_c) \rangle_V, \quad (8)$$

and for the typical medium:

(2) Typical average (TMT):

$$\underline{G}_{typ}^{LIZ}(\omega) = e^{1/N_c \sum_{I_c} \langle \ln [\rho_{I_c, I_c}(\omega, V, I_c)] \rangle_V} \times \frac{1}{N_c} \sum_{I_c} \left\langle \frac{\underline{G}^{LIZ}(\omega, V, I_c)}{\rho_{I_c, I_c}(\omega, V, I_c)} \right\rangle_V, \quad (9)$$

where the density $\rho_{I_c, I_c}(\omega, V, I_c)$ is the density at the center of the LIZ defined as

$$\rho_{I_c, I_c}(\omega, V, I_c) = -\frac{1}{\pi} \text{Im}[\underline{G}^{LIZ}(\omega, V, I_c)]_{I_c, I_c}. \quad (10)$$

To obtain the typical value, we perform a geometric average of the local density of states at the center of the LIZ over all the LIZs and disorder configurations, which is expressed as the exponential term in Eq. (9), while the second multiplicative term of Eq. (9) is a linear average of the whole LIZ Green's function that is normalized by the density of states at its center.

In Fig. 3 we present the self-consistency loop for both CPA and TMT embeddings as described above. The central

quantity to be iterated within the self-consistent calculation is the local effective self-energy $\Sigma_l(\omega)$. This can be computed as

$$\Sigma_l(\omega) = [\underline{g}^{-1}(\omega)]_{I_c, I_c} - [\underline{G}_{ave, (typ)}^{LIZ-1}(\omega)]_{I_c, I_c}, \quad (11)$$

where $\underline{G}_{ave, (typ)}^{LIZ}(\omega)$ is the disorder-averaged $\underline{G}^{LIZ}(\omega, V)$. When constructing the typical Green's function for the TMT embedding, we replace $\underline{G}_{ave}^{LIZ}(\omega)$ by $\underline{G}_{typ}^{LIZ}(\omega)$ in the calculation of the local self-energy $\Sigma_l(\omega)$ [Eq. (11)]. In Eq. (9), the sum is over the sites I_c in the supercell. The typical Green's function is constructed in the spirit that its imaginary part gives the geometric average of the LDOS for the central sites in all the LIZs in all the disorder configurations. This quantity, called the TDOS, serves as an order parameter to describe the localization transition [55]. In the limit of weak disorder the difference between the TDOS and the normal DOS is negligible and Eq. (9) reduces to the normal averaged Green's function, Eq. (8); consequently, the TMT embedding reduces to the CPA embedding.

The coarse-graining procedure of Eq. (3) is due to the fact that the supercell is effectively embedded in the same effective medium as the LIZ. For the case of supercell size $N_c = 1$, Eq. (3) reduces to the local (momentum independent) Green's function. In this case N_{LIZ} will also reduce to 1; therefore, the LIZ Green's function from Eq. (1) also becomes local. Consequently, our method reduces to CPA or TMT depending on how we perform the disorder averaging.

Note that a full matrix inversion is required only within the LIZ. Thus, both the CPA and the TMT-based LIZ algorithms scale like $N_c N_{LIZ}^3$, where the prefactor is due to the need to solve Eq. (11) at the LIZ centered on every site in the system. In the TMDCA formalism, the calculation scales as N_c^3 . Since $N_{LIZ} \ll N_c$, the proposed embedding method significantly reduces the computational cost compared to TMDCA.

V. RESULTS

In the following we apply the above embedding method to the single-band 3D Anderson model with the Hamiltonian:

$$H = -t \sum_{\langle ij \rangle \sigma} (c_{i\sigma}^\dagger c_{j\sigma} + \text{H.c.}) + \sum_{i\sigma} V_i n_{i\sigma}. \quad (12)$$

The first term describes electrons with spin σ , hopping with the amplitude t , between sites i and j (only nearest-neighbor hopping is included). The second term describes static scattering processes on the local disorder center. The local potential V_i is modeled as the random number drawn from a uniform box distribution, $p(V) = \frac{1}{2W} \Theta(W - |V|)$. By the condition $4t = 1$ the energy units are fixed. In the calculation, we choose cubic supercells of size $N_c = L_c^3$. The corresponding LIZ volumes are also of cubic shape with size $N_{LIZ} = L_{LIZ}^3$. The calculations were performed for a total of 400 disorder realizations with the proper disorder averaging. Calculations are performed in the thermodynamic limit despite the finite size of the LIZ. This is a consequence of the fact that the supercell containing LIZ is embedded into an effective medium. Note that embedding schemes lead to faster convergence rates in size for both supercells as well as for LIZs [40].

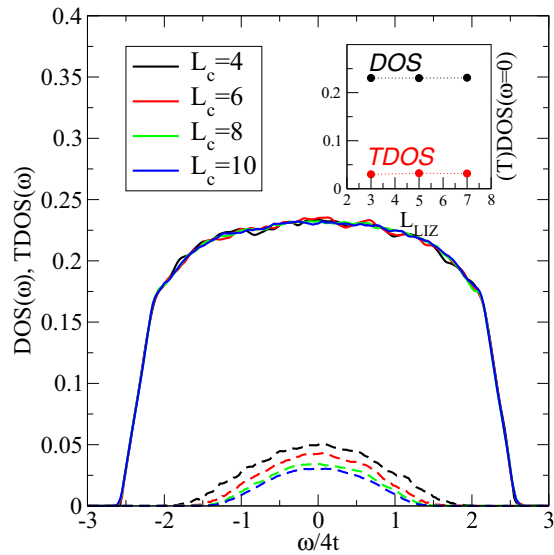


FIG. 4. Comparison of the average DOS (solid curves) and the typical TDOS (dashed curves) at different supercell sizes $L_c = 4, 6, 8, 10$ with fixed LIZ size $L_{LIZ} = 3$. The disorder strength is set to be $W = 2.0$. Inset: Comparison of DOS and TDOS at the band center with supercell size $L_c = 10$ and three different LIZ sizes: 3, 5, and 7. They are independent of the size of the LIZ.

Figure 4 shows the comparison of average and typical DOS for different supercell sizes. We also plot in the inset the DOS and TDOS at the band center as a function of the LIZ size. As the size increases from 3 to 7 both DOS and TDOS remain almost unchanged; therefore, in the following we will show only results obtained for $L_{LIZ} = 3$.

The other relevant length scale is the size of the supercell L_c . We performed calculations for different supercell sizes keeping fixed $L_{LIZ} = 3$, as shown in the main panel of Fig. 4. As can be seen, DOS results show no significant change for different supercell sizes. On the contrary, the magnitude of TDOS decreases slowly with the increase of the supercell size L_c . Since the TDOS defines the order parameter of the Anderson localization, it vanishes at the critical transition point [5]. In order to compute the value of the critical disorder strength W_c for each supercell, we extrapolate linearly the values of TDOS at the band center towards zero. Data to be extrapolated are taken from calculations performed for sets of disorder strengths in the vicinity of the critical value $W_c \approx 2.1$ [42–49].

In the following we investigate how effective the typical embedding scheme is in capturing Anderson localization as a consequence of strong disorder. In Fig. 5, we plot the $\text{TDOS}(\omega = 0)$ at the band center as a function of disorder strength W . The Anderson transition is then defined by vanishing $\text{TDOS}(\omega = 0)$ above the critical disorder strength W_c . We can do a further extrapolation of W_c vs $1/L_c$ to estimate the critical disorder strength W_c in the thermodynamic limit. This is shown in the inset of Fig. 5. The extrapolated value $W_c = 2.09$ turns out to be in excellent agreement with the exact results $W_c \approx 2.10$ [42–49]. The other quantity that is also sensitive to the localization physics is the inverse participation ratio. The typical value of this quantity was studied in the

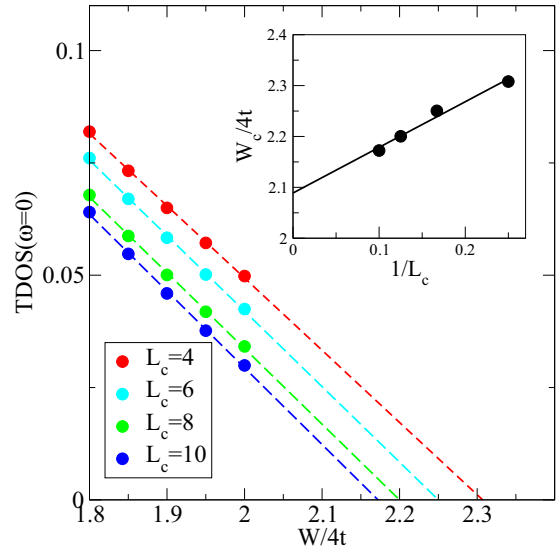


FIG. 5. Extrapolation of TDOS at the band center as a function of disorder strength W for various supercell sizes with fixed LIZ size $L_{LIZ} = 3$. Inset: extrapolation of the critical disorder strength W_c to the thermodynamic limit.

finite size system which shows a critical behavior close to the transition region upon a finite size scaling [65]. We also calculate the generalized inverse participation ratio in our TMT embedding method; as shown in the Appendix, it has the similar behavior as that in Ref. [65] and also captures the localization physics.

In conclusion, we have developed a method for disordered systems, which takes advantage of a LIZ construction to efficiently compute the local Green's function corresponding to a supercell embedded into an effective medium. We apply this method to a single-band 3D Anderson model. For a typical effective medium embedding of the supercell we are able to capture the physics of Anderson localization. The numerical extrapolation predicts an accurate critical disorder strength for the localization transition. We find the embedding method has a quick convergence as the LIZ size, and hence reduces the computational effort.

The present method may serve as a guide for developing an efficient typical medium embedding scheme in the multiple-scattering framework. Eventually, this allows first-principles studies of the localization effects in functional materials containing disorder.

ACKNOWLEDGMENTS

This paper is based upon work supported by the US Department of Energy, Office of Science, Office of Basic Energy Sciences under Award No. DE-SC0017861. This work used the high performance computational resources provided by the Louisiana Optical Network Initiative, and HPC@LSU computing. The work of M.E. has been supported by US Department of Energy, Office of Science, Basic Energy Sciences, Material Sciences and Engineering Division and it used resources of the Oak Ridge Leadership Computing Facility, which is a DOE Office of Science User Facility supported under Contract No. DE-AC05-00OR22725. L.C. gratefully

acknowledges the financial support offered by the Augsburg Center for Innovative Technologies, and by the Deutsche Forschungsgemeinschaft (DFG, German Research Foundation), Project No. 107745057-TRR 80/F6.

APPENDIX: BEHAVIOR OF THE GENERALIZED INVERSE PARTICIPATION RATIO

We also calculate the generalized inverse participation ratio using Eq. (1) of Ref. [65].

$$G_2(\omega) = \frac{\sum_{I_c} \rho_{I_c}(\omega, I_c)^2}{\left[\sum_{I_c} \rho_{I_c}(\omega, I_c)\right]^2}. \quad (\text{A1})$$

$G_2(\omega)$ is obtained in the last step after the self-consistency loop convergence is reached and the summation of I_c goes over the whole supercell. We calculate the typical value of $G_2(\omega)$ at the band center using Eq. (16) of Ref. [65].

$$G_2^{typ}(\omega) = \exp[(\ln G_2(\omega))_V], \quad (\text{A2})$$

where the geometric average is done over the disorder configurations. The results are shown in Fig. 6, and are similar to those of Fig. 4(a) of Ref. [65]. For the weak disorder case, the slope is close to a constant, while for the strong disorder case, the slope decreases as the supercell size increases, which

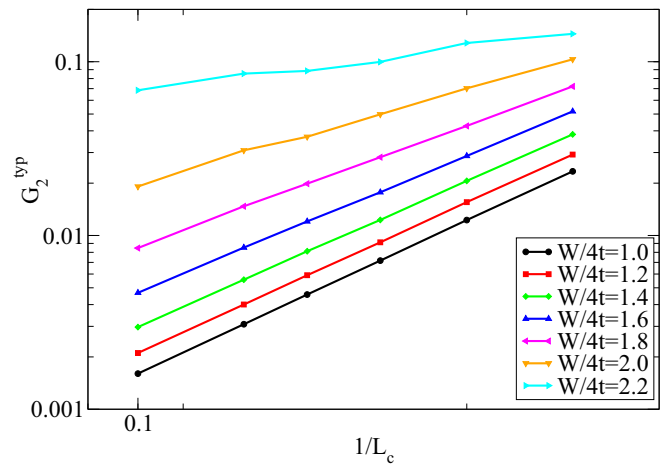


FIG. 6. The typical generalized inverse participation ratio calculated using the typical medium embedding formalism as a function of supercell size, with various disorder strength. The supercell sizes used are $L_s = 4, 5, 6, 7, 8, 10$ and the LIZ size is fixed with $L_{LIZ} = 3$.

is consistent with the behavior of the localized states. This further justifies that our method can capture the localization physics.

-
- [1] *50 Years of Anderson Localization*, edited by E. Abrahams (World Scientific, Singapore, 2010).
- [2] R. J. Elliott, J. A. Krumhansl, and P. L. Leath, *Rev. Mod. Phys.* **46**, 465 (1974).
- [3] D. Belitz and T. R. Kirkpatrick, *Rev. Mod. Phys.* **66**, 261 (1994).
- [4] D. Vollhardt, *Rev. Mod. Phys.* **56**, 99 (1984).
- [5] H. Terletska, Y. Zhang, K.-M. Tam, T. Berlijn, L. Chioncel, N. S. Vidhyadhiraja, and M. Jarrell, *Appl. Sci.* **8**, 2401 (2018).
- [6] P. W. Anderson, *Phys. Rev.* **109**, 1492 (1958).
- [7] M. M. Radonjić, D. Tanasković, V. Dobrosavljević, and K. Haule, *Phys. Rev. B* **81**, 075118 (2010).
- [8] M. Neupane, S.-Y. Xu, R. Sankar, N. Alidoust, G. Bian, C. Liu, I. Belopolski, T.-R. Chang, H.-T. Jeng, H. Lin, A. Bansil, F. Chou, and M. Z. Hasan, *Nat. Commun.* **5**, 3786 (2014), article.
- [9] Z. K. Liu, B. Zhou, Y. Zhang, Z. J. Wang, H. M. Weng, D. Prabhakaran, S.-K. Mo, Z. X. Shen, Z. Fang, X. Dai, Z. Hussain, and Y. L. Chen, *Science* **343**, 864 (2014).
- [10] S. Borisenko, Q. Gibson, D. Evtushinsky, V. Zabolotnyy, B. Büchner, and R. J. Cava, *Phys. Rev. Lett.* **113**, 027603 (2014).
- [11] Z. K. Liu, J. Jiang, B. Zhou, Z. J. Wang, Y. Zhang, H. M. Weng, D. Prabhakaran, S.-K. Mo, H. Peng, P. Dudin, T. Kim, M. Hoesch, Z. Fang, X. Dai, Z. X. Shen, D. L. Feng, Z. Hussain, and Y. L. Chen, *Nat. Mater.* **13**, 677 (2014).
- [12] B. Q. Lv, H. M. Weng, B. B. Fu, X. P. Wang, H. Miao, J. Ma, P. Richard, X. C. Huang, L. X. Zhao, G. F. Chen, Z. Fang, X. Dai, T. Qian, and H. Ding, *Phys. Rev. X* **5**, 031013 (2015).
- [13] S.-Y. Xu, I. Belopolski, N. Alidoust, M. Neupane, G. Bian, C. Zhang, R. Sankar, G. Chang, Z. Yuan, C.-C. Lee, S.-M. Huang, H. Zheng, J. Ma, D. S. Sanchez, B. Wang, A. Bansil, F. Chou, P. P. Shibayev, H. Lin, S. Jia, and M. Z. Hasan, *Science* **349**, 613 (2015).
- [14] S.-Y. Xu, N. Alidoust, I. Belopolski, Z. Yuan, G. Bian, T.-R. Chang, H. Zheng, V. N. Strocov, D. S. Sanchez, G. Chang, C. Zhang, D. Mou, Y. Wu, L. Huang, C.-C. Lee, S.-M. Huang, B. Wang, A. Bansil, H.-T. Jeng, T. Neupert, A. Kaminski, H. Lin, S. Jia, and M. Zahid Hasan, *Nat. Phys.* **11**, 748 (2015).
- [15] N. F. Mott, *Adv. Phys.* **16**, 49 (1967).
- [16] N. F. Mott, *Rev. Mod. Phys.* **40**, 677 (1968).
- [17] T. Ying, Y. Gu, X. Chen, X. Wang, S. Jin, L. Zhao, W. Zhang, and X. Chen, *Sci. Adv.* **2**, e1501283 (2016).
- [18] P. Hohenberg and W. Kohn, *Phys. Rev.* **136**, B864 (1964).
- [19] W. Kohn and L. J. Sham, *Phys. Rev.* **140**, A1133 (1965).
- [20] W. Kohn, *Rev. Mod. Phys.* **71**, 1253 (1999).
- [21] R. O. Jones and O. Gunnarsson, *Rev. Mod. Phys.* **61**, 689 (1989).
- [22] R. O. Jones, *Rev. Mod. Phys.* **87**, 897 (2015).
- [23] P. Soven, *Phys. Rev.* **156**, 809 (1967).
- [24] J. Koringa, *Physica* **13**, 392 (1947).
- [25] W. Kohn and N. Rostoker, *Phys. Rev.* **94**, 1111 (1954).
- [26] G. M. Stocks, R. W. Williams, and J. S. Faulkner, *Phys. Rev. B* **4**, 4390 (1971).
- [27] O. K. Andersen, *Phys. Rev. B* **12**, 3060 (1975).
- [28] J. Kudrnovský, V. Drchal, and J. Masek, *Phys. Rev. B* **35**, 2487 (1987).
- [29] J. Kudrnovský and V. Drchal, *Phys. Rev. B* **41**, 7515 (1990).
- [30] I. Abrikosov, Y. Vekilov, and A. Ruban, *Phys. Lett. A* **154**, 407 (1991).
- [31] I. A. Abrikosov and H. L. Skriver, *Phys. Rev. B* **47**, 16532 (1993).

- [32] O. K. Andersen, O. Jepsen, and G. Krier, *Lectures on Methods of Electronic Structure Calculation* (World Scientific, Singapore, 1994).
- [33] L. Vitos, *Phys. Rev. B* **64**, 014107 (2001).
- [34] L. Vitos, *Computational Quantum Mechanics for Materials Engineers* (Springer, London, 2010).
- [35] L. Vitos, J. Kollár, and H. L. Skriver, *Phys. Rev. B* **49**, 16694 (1994).
- [36] L. Vitos, I. A. Abrikosov, and B. Johansson, *Phys. Rev. Lett.* **87**, 156401 (2001).
- [37] R. Car and M. Parrinello, *Phys. Rev. Lett.* **55**, 2471 (1985).
- [38] M. C. Payne, M. P. Teter, D. C. Allan, T. A. Arias, and J. D. Joannopoulos, *Rev. Mod. Phys.* **64**, 1045 (1992).
- [39] Y. Wang, G. M. Stocks, W. A. Shelton, D. M. C. Nicholson, Z. Szotek, and W. M. Temmerman, *Phys. Rev. Lett.* **75**, 2867 (1995).
- [40] I. A. Abrikosov, A. M. N. Niklasson, S. I. Simak, B. Johansson, A. V. Ruban, and H. L. Skriver, *Phys. Rev. Lett.* **76**, 4203 (1996).
- [41] I. A. Abrikosov, S. I. Simak, B. Johansson, A. V. Ruban, and H. L. Skriver, *Phys. Rev. B* **56**, 9319 (1997).
- [42] K. Slevin and T. Ohtsuki, *Phys. Rev. Lett.* **82**, 382 (1999).
- [43] B. Bulka, B. Kramer, and A. MacKinnon, *Z. Phys. B* **60**, 13 (1985).
- [44] G. Schubert, A. Weibe, G. Wellin, and H. Fehske, *High Performance Computing in Sci. and Engineering, Garching 2004* (Springer, New York, 2005), pp. 237–249.
- [45] Y. Song, W. A. Atkinson, and R. Wortis, *Phys. Rev. B* **76**, 045105 (2007).
- [46] K. Slevin and T. Ohtsuki, *Phys. Rev. B* **63**, 045108 (2001).
- [47] A. Rodriguez, L. J. Vasquez, K. Slevin, and R. A. Römer, *Phys. Rev. Lett.* **105**, 046403 (2010).
- [48] A. Rodriguez, L. J. Vasquez, K. Slevin, and R. A. Römer, *Phys. Rev. B* **84**, 134209 (2011).
- [49] A. MacKinnon and B. Kramer, *Phys. Rev. Lett.* **47**, 1546 (1981).
- [50] M. Eisenbach, J. Larkin, J. Lutjens, S. Rennich, and J. H. Rogers, *Comput. Phys. Commun.* **211**, 2 (2017).
- [51] Y. Yang, C.-C. Chen, M. C. Scott, C. Ophus, R. Xu, A. Pryor, L. Wu, F. Sun, W. Theis, J. Zhou, M. Eisenbach, P. R. C. Kent, R. F. Sabirianov, H. Zeng, P. Ercius, and J. Miao, *Nature (London)* **542**, 75 (2017).
- [52] D. D. Johnson and F. J. Pinski, *Phys. Rev. B* **48**, 11553 (1993).
- [53] F. J. Pinski, *Phys. Rev. B* **57**, 15140 (1998).
- [54] B. Ujfalussy, J. S. Faulkner, N. Y. Moghadam, G. M. Stocks, and Y. Wang, *Phys. Rev. B* **61**, 12005 (2000).
- [55] V. Dobrosavljević, A. A. Pastor, and B. K. Nikolić, *Europhys. Lett.* **62**, 76 (2003).
- [56] G. Schubert, J. Schleede, K. Byczuk, H. Fehske, and D. Vollhardt, *Phys. Rev. B* **81**, 155106 (2010).
- [57] M. Jarrell and H. R. Krishnamurthy, *Phys. Rev. B* **63**, 125102 (2001).
- [58] H. Terletska, C. E. Ekuma, C. Moore, K.-M. Tam, J. Moreno, and M. Jarrell, *Phys. Rev. B* **90**, 094208 (2014).
- [59] Y. Zhang, H. Terletska, C. Moore, C. Ekuma, K.-M. Tam, T. Berlijn, W. Ku, J. Moreno, and M. Jarrell, *Phys. Rev. B* **92**, 205111 (2015).
- [60] Y. Zhang, R. Nelson, E. Siddiqui, K.-M. Tam, U. Yu, T. Berlijn, W. Ku, N. S. Vidhyadhiraja, J. Moreno, and M. Jarrell, *Phys. Rev. B* **94**, 224208 (2016).
- [61] C. E. Ekuma, V. Dobrosavljević, and D. Gunlycke, *Phys. Rev. Lett.* **118**, 106404 (2017).
- [62] Y. Zhang, R. Nelson, K.-M. Tam, W. Ku, U. Yu, N. S. Vidhyadhiraja, H. Terletska, J. Moreno, M. Jarrell, and T. Berlijn, *Phys. Rev. B* **98**, 174204 (2018).
- [63] H. Terletska, Y. Zhang, L. Chioncel, D. Vollhardt, and M. Jarrell, *Phys. Rev. B* **95**, 134204 (2017).
- [64] Note, however, that within LSMS no such requirement is necessary; even a single site can be considered as supercells for a specific large LIZ.
- [65] N. C. Murphy, R. Wortis, and W. A. Atkinson, *Phys. Rev. B* **83**, 184206 (2011).